THE JOURNAL OF PHYSICAL CHEMISTRY C
A JOURNAL OF THE AMERICAN CHEMICAL SOCIETY

pubs.acs.org/JPCC

Article

Etching-Free Transfer and Nanoimaging of CVD-Grown MoS_2 Monolayers

Syed Hamza Safeer, Thiago L. Vasconcelos, Bruno S. Oliveira, Braulio Soares Archanjo, Michael Nazarkovsky, Cecília Vilani, Fernando Lazaro Freire, and Victor Carozo*

Cite This: *J. Phys. Chem. C* 2021, 125, 21011–21017

Read Online

ACCESS | Metrics & More | Article Recommendations | Supporting Information

ABSTRACT: The transfer of two-dimensional materials from grown substrates onto target substrates is critical for device applications and postgrown analysis. The traditional transfer method for as-grown two-dimensional materials requires a wet chemical etching process that damages the crystals and the substrates. These issues deteriorate the electrical and optical performances of two-dimensional-material-based devices fabricated afterward. Herein, we developed an etching-free method and nanoimaging for transferring and analyzing monolayers of MoS_2 onto arbitrary substrates using polyurethane as a sacrifice polymer. The polymer layer and the MoS_2 crystals can be peeled off from the substrate by tweezers and transferred to any substrate. We analyzed the transferred samples to a glass coverslip substrate with optical microscopy, atomic force microscopy, tip-enhanced Raman spectroscopy, and tip-enhanced photoluminesce spectroscopy. Also, we transferred monolayers of MoS_2 to a transmission electron microscopy grid and acquired scanning electron microscopy together with high-resolution scanning transmission electron microscopy images. The results of nanoimaging indicate that the method preserved the sample's optical and structural properties and avoid undesirable cracks, wrinkles, and polymer residues. The etching-free transfer method of as-grown two-dimensional materials will improve the quality of transferred samples enhance the devices' performance.

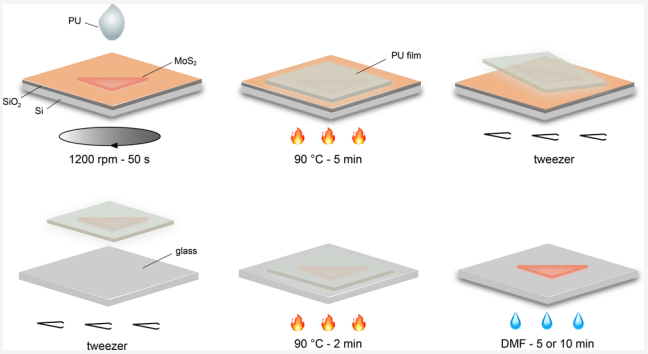

INTRODUCTION

The discovery of graphene and other two-dimensional (2D) materials has opened an entirely new field of research in material science.[1−8] They became the most studied materials over the past decade. The monolayers of transition metal dichalcogenides (TMD) have a direct bandgap, which makes them promising candidates for optical and nanoelectronics devices.[9−15] There are many techniques capable of obtaining monolayers of 2D-TMD, from which the most straightforward is the mechanical exfoliation of bulk crystals.[16−18] However, this approach is not reproducible and scalable. Also, it has some limitations regarding shape, size, and problems during the transfer procedure. These facts may impair the performance of 2D-TMD-based devices.[19]

Chemical vapor deposition (CVD) is the most promising technique to obtain large monolayers of 2D-TMD materials for practical applications. However, there are drawbacks regarding the as-grown samples. 2D-TMD are synthesized at high temperatures ~850 °C usually on SiO_2/Si substrates.[20−25] The high synthesis temperature damages the substrate and causes the leakage current in the devices. For many other applications, those 2D-TMD need to be retrieved and placed onto target substrates. For example, to study transmission properties, flexible devices, and achieve artificially stacked bilayers, postgrowth transfer of 2D-TMD from the growth substrate is usually needed. In the CVD synthesis technique, a strain is introduced during the growth and cooling processes due to the difference in thermal expansion coefficients between 2D-TMD and the substrate.[26] Thus, a postgrowth transfer is inevitable for characterization and device applications.

Unlike exfoliation from the bulk, it is impossible to peel off and transfer a CVD-grown 2D-TMD by mechanical exfoliation method.[27] The most widely used approach for transferring CVD-grown 2D-TMD onto arbitrary substrates is the wet transfer using poly(methyl methacrylate) (PMMA). This method involves the spin-coating of a PMMA support layer and subsequent etching of the substrate in an alkaline solution containing NaOH or KOH.[28−30] The PMMA is dissolved in acetone after the transfer. Immersing a thin 2D-TMD sample

Received: June 22, 2021
Published: September 16, 2021

https://doi.org/10.1021/acs.jpcc.1c05510
J. Phys. Chem. C 2021, 125, 21011–21017

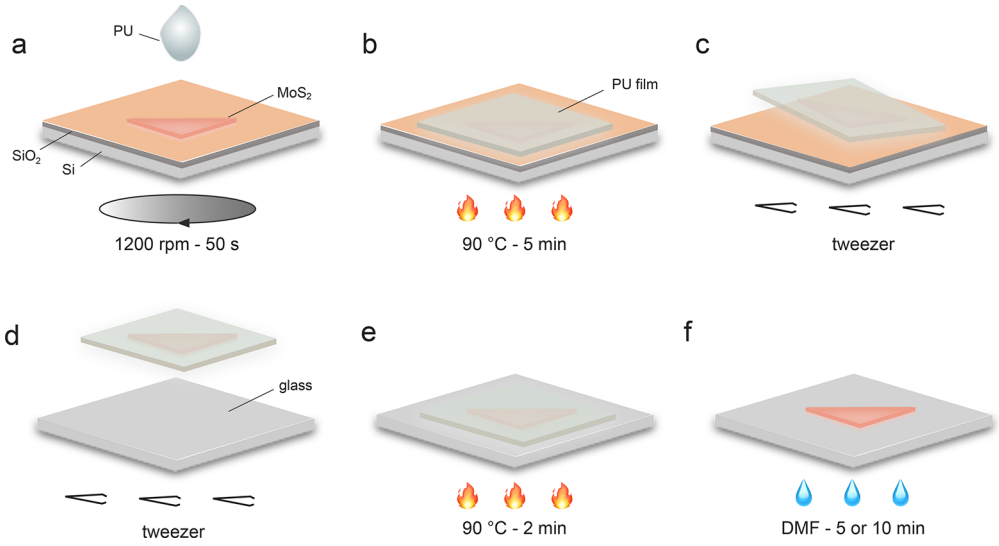

Figure 1. Scheme of etching-free transfer procedure using polyurethane. (a) Drop a polyurethane solution on the sample and spin coating using 1200 rpm for 50 s. (b) Heat the sample on a hot plate for 5 min at 90 °C. (c) Peel off the polyurethane layer along with 2D-TMD crystals using the tweezers. (d) Transfer the polyurethane layer with the 2D-TMD to the coverslip substrate. (e) Heat the sample on a hot plate for 2 min at 90 °C. (f) Dissolve the polyurethane layer using DMF.

into acetone for a long time can cause severe structural damage to the crystal. The etching process and acetone exposition leave cracks, wrinkles, and polymer residues on the transferred 2D-TMD, which degrade the electrical and optical properties of 2D-TMD.[31−33]

Recently, several alternative transfer approaches have been developed to overlay these issues.[33−40] For example, a transfer method using water-soluble polymer (polyvinylpyrrolidone) and poly(vinyl alcohol) was tested.[39] These polymers are not adhesive and flexible, making it difficult to peel off the polymer layer after spin coating. On the other hand, polyurethane is an adhesive and flexible polymer. The polyurethane can be dissolved in dimethylformamide (DMF), not damaging the 2D TMD structure. Additionally, uniform polyurethane films formed after a solvent evaporates are resoluble and removed from a spot. The preferred solvent for polyurethane must not interact with 2D-TMD. The compatibility of polyurethane with other nanomaterials is reflected in various publications.[41−45] Hence, a simple, nondestructive, etching-free transfer method for as-grown 2D-TMD has not been well established yet, and polyurethane can be a candidate for the sacrifice polymer layer.

This manuscript describes an etching-free transfer method and a nanoimaging of as-grown monolayers of MoS_2. We transferred samples to a glass coverslip and to a transmission electron microscopy (TEM) grid to evaluate the method. We used optical microscopy, atomic force microscopy (AFM), tip-enhanced Raman spectroscopy (TERS), and tip-enhanced photoluminesce spectroscopy (TEPL) to analyze the surface and the optical properties of the sample on the coverslip substrate. Also, we acquired scanning electron microscopy (SEM) and high-resolution scanning transmission electron microscopy (HRSTEM) images to analyze the crystallinity of post-transferred samples. Based on our observations, the as-grown monolayers of MoS_2 transferred maintain their optical and structural properties, and they are free from cracks, wrinkles, and polymer residues. Our analysis suggests that the etching-free method can transfer as-grown 2D materials to any arbitrary substrates.

MATERIALS AND METHODS

Chemical Vapor Deposition. We utilized the atmospheric pressure chemical vapor deposition (APCVD) technique to obtain monolayers of MoS_2. MoO_3 (8−10 mg, Sigma-Aldrich, 99.99% purity) was loaded in an alumina crucible. Then 350 mg of sulfur fine powder (Sigma-Aldrich, 99.5% purity) was loaded in another aluminum crucible. The synthesis was carried out inside a quartz tube in a dual-zone tubular furnace. We used the argon flow rate at 100 sccm. The heating in the furnace was programmed at the rate of 33 °C/min until it reaches 850 °C for MoO_3 powder and 250 °C for sulfur powder. We kept the materials under the respective constant temperatures for the next 15 min and then cooled them down naturally. Figure S1 shows the scheme of the APCVD setup. More details can be found in ref 25.

Preparation of the Polyurethane Solution. We used polyurethane (Elastollan R 1185 A, TPU) purchased from BASF Polyurethanes in the present study. To prepare a concentrated polyurethane solution, we dissolved 1 g of polyurethane in 15 mL of *N*-dimethylformamide and mixed it for 24 h by the magnetic spinner. Freshly prepared solutions were used during the whole study.

Atomic Force Microscopy. The contact mode AFM was applied to measure the thickness of the transferred MoS_2 using the NT-MDT (High-End AFM-nano-Raman/IR Equipment) equipment with a 10 × 10 μm^2 piezoelectric stage. The measurement was taken in contact mode by using a silicon tip with gold on top.

Raman and Photoluminescence Spectroscopy. The Raman and photoluminescence maps and spectra were acquired using a micro-Raman spectrometer (NT-MDT, NTEGRA SPECTRA) in a backscattering configuration equipped with a solid-state laser (473 nm). We carried out the experiments using a 100× objective and an incident laser power of 0.2 mW. We collected the Raman and PL mapping images using a 10 × 10 μm^2 piezoelectric stage.

Tip-Enhanced Raman Spectroscopy and Tip-Enhanced Photoluminesce Spectroscopy. The TERS and TEPL experimental setup used in the current work was similar

https://doi.org/10.1021/acs.jpcc.1c05510
J. Phys. Chem. C 2021, 125, 21011−21017

to that described in detail in ref 46. The system was based on an inverted optical microscope (bottom illumination), and a high numerical aperture objective lens (1.4 NA) was used to focus a radially polarized HeNe laser beam (λ_{laser} = 632.8 nm) on the substrate's surface. A homemade shear-force-based AFM held a plasmon-tunable tip pyramid (PTTP) nanoantenna close to the sample to collect the near-field information with high optical efficiency and overcome the diffraction limit of light.[47−49] For the TERS spectral image acquisition, the laser power at the objective entrance was ∼190 μW. The image width was 5 μm (2 μm), and the pixel size was around 39.06 nm (31.25 nm), with an integration time of 0.3 s (1.0 s) for the first (second) experiment shown in Figures 3c and 3d,i, respectively. The tip-down/tip-up spectra shown in Figure 3b were collected with five accumulations of 10 s.

High-Resolution Scanning Transmission Electron Microscopy. MoS_2 triangular flakes were transferred to a conventional holey carbon Cu grid with 300 mesh. The transfer was assisted by a polyurethane polymer film with the same procedure as the transfer on coverslip substrates. The scanning transmission electron microscopy (STEM) imaging was performed at the acceleration voltage of 80 kV and 50 pA current in a probe corrected FEI Titan 80-300 using a high-angle annular dark-field detector (HAADF).

RESULTS AND DISCUSSION

To transfer the as-grown MoS_2 monolayers onto a glass coverslip substrate, we first placed the SiO_2/Si substrate in the spin coater. We put a tape at the corner of the sample to peel off the polyurethane film later. We dropped a polyurethane solution, and the substrate was then rotated at speed up to 1200 rpm for 50 s (see Figure 1a) to deposit a uniform polyurethane thin film. The thickness formed was ∼80 nm. Then, the sample was heated on a hot plate for 5 min at 90 °C, Figure 1b. Polyurethane is adhesive and forms high-strength bonds with the 2D-TMD crystals after drying. Next, the polyurethane layer and the MoS_2 crystals were peeled off from the substrate by tweezers due to the solid polyurethane−sample interactions; see Figure 1c. The polyurethane layer was then transferred to the glass coverslip substrate, Figure 1d, and heated again on a hot plate at 90 °C for 2 min, Figure 1e. Finally, the polyurethane layer was submerging in DMF for 5−10 min (see Figure 1f), and we have the MoS_2 crystals on the new substrate (see photographs of the steps in Figure S2).

Polyurethane is highly soluble in DMF and does not tear down or damage the MoS_2 samples. Figures 2a and 2b show the as-grown monolayers of MoS_2 before and after the transfer. The crystals of the region (a) are on the coverslip. The optical images of the MoS_2 sample on glass demonstrated clean transfer with no residual polyurethane left, and the triangular shape was preserved. The AFM examined the surface of the transferred MoS_2. Figure 2c shows the AFM topography image of a transferred MoS_2 sample demonstrating a uniform surface. The line profile indicates the thickness around 1 nm, thus confirming the complete dissolution of the polyurethane polymer film. Far-field Raman and PL spectra were taken before and after; see Figures 2d and 2e. The structural and electronic characteristics were preserved, and we did not find any signal of polymers. In Figures S3, S4, S5, and S6 we show additional transferred samples. These results confirmed the repeatability of the etching-free method.

TERS and TEPL were applied to investigate the transferred samples' optical property and surface at the nanoscale. The far-field photoluminescence (PL) imaging, Figure 3a, was made with an avalanche photodiode (APD) using a bandpass filter centered at 1.80 eV, selecting a spectral window roughly between 1.82 and 1.78 eV, on which the color scale renders the PL intensity. The selected MoS_2 flake is a triangular monolayer with 20 μm of lateral size. The spectra in Figure 3b were collected at the position indicated with a black cross at Figure 3a, with (orange) and without (black) the PTTP nanoantenna, where we measured a Raman spectral enhancement of ∼17× (A'_{1g} peak) and PL enhancement of ∼5× (1.91 eV). This high spectral enhancement generated by the PTTP nanoantenna with localized surface plasmon tuned at the laser wavelength was necessary to generate the high near-field to far-field imaging contrast.[47,48] The PTTP nanoantenna was designed to be optically efficient at around 1.96 eV. Thus, the near-field spectrum observed in Figure 3b presents a more intense tail at the high energy side (>1.85 eV) when compared to the lower energy side (<1.75 eV). Spatially, a more substantial PL contribution is observed close to the triangle vertices (see the white dashed square inset on Figure 3a). At that one, we performed a TEPL hyperspectral imaging, seen in Figure 3c, with color rendering the intensity centered at 1.8 eV. The white dashed square inset at the Figure 3c indicates the area where the other TERS and TEPL hyperspectral images were acquired. The AFM topography image acquired simultaneously during TEPL and TERS can be found in Figure 3d.

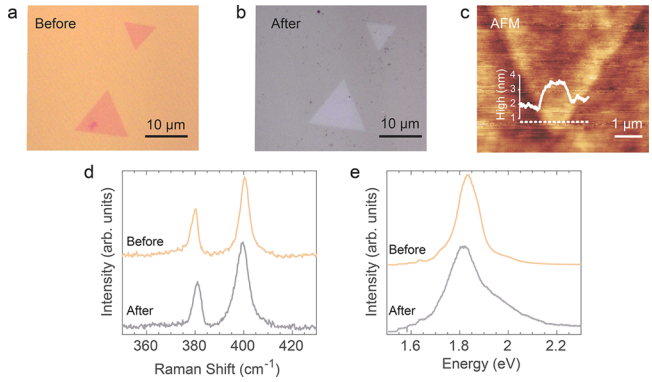

Figure 2. Optical and spectroscopy analysis of the MoS_2 monolayer before and after. (a) Optical image of as-grown monolayers of MoS_2 on SiO_2 substrate. (b) Optical image of the MoS_2 crystals transferred to a coverslip. (c) AFM topography image of a monolayer on the coverslip. (d, e) Raman and PL spectra before and after.

Figure 3e presents a hyperspectral TEPL intensity image of neutral exciton at 1.80 eV. Figure 3f is a plot of TEPL spectra (black), and the fitting (orange) for two points is shown in Figure 3e. We used a unique Gaussian function to adjust the spectra because the neutral and trion excitons could not be distinguish. Trions have a low or absent intensity in the PL spectrum taken at room temperature.[50] Figures 3g and 3h are respectively the TEPL spectral peak position and the TEPL peak full width of half-maximum (fwhm). These TEPL images combined with the AFM image suggest that few dark points of reduced PL intensity are likely related to some synthesis residue laid at its surface. These residues seem to quench the PL where they are present by moving the PTTP nanoantenna away from the sample few nanometers, resulting in a decrease in the near-field contribution and the TEPL intensity on these points. Since we could not observe any Raman signature from polymers on those sites (the polyurethane has Raman signatures around 1200 cm^{-1} [41]), they are probably synthesis

https://doi.org/10.1021/acs.jpcc.1c05510
J. Phys. Chem. C 2021, 125, 21011−21017

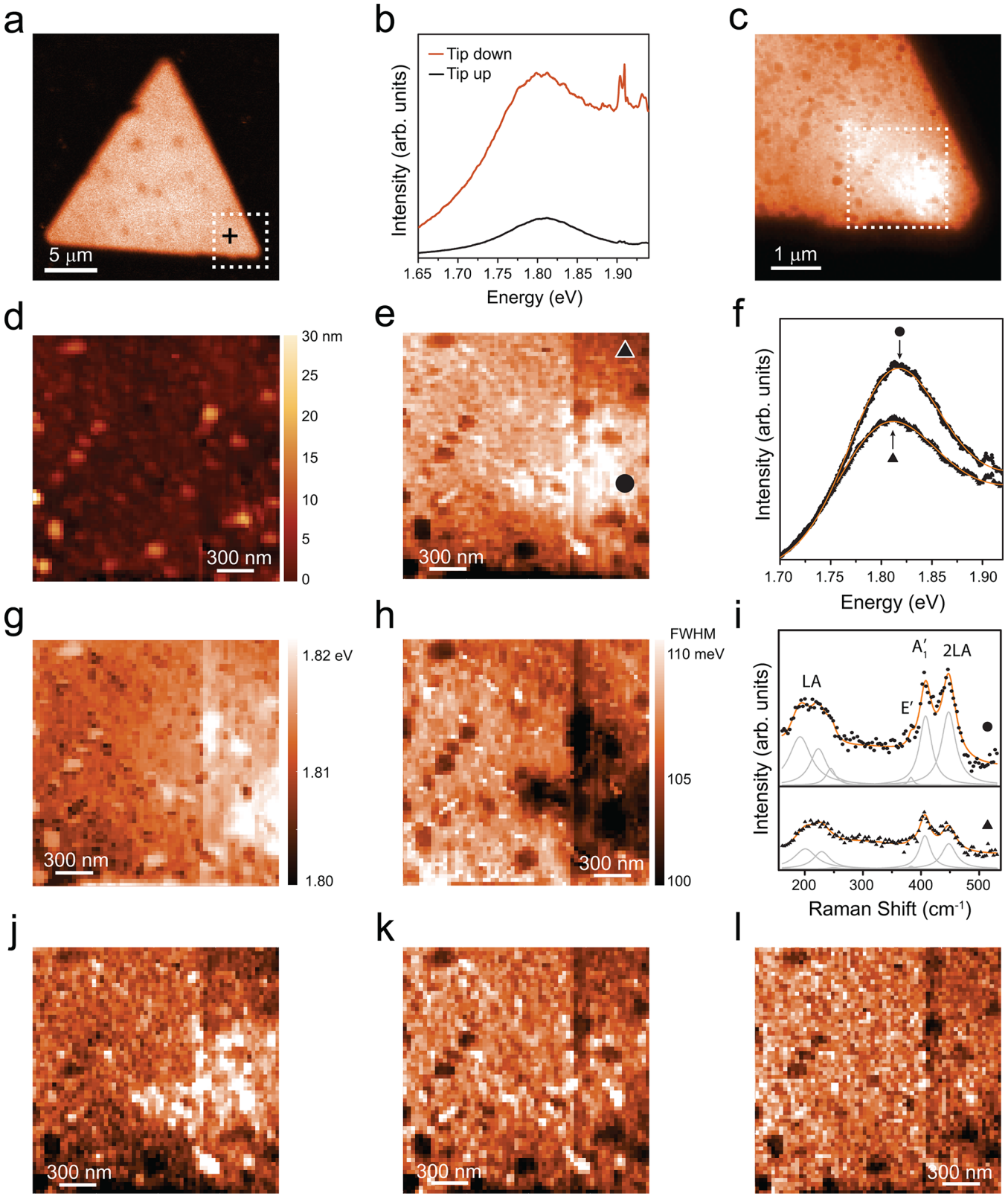

Figure 3. TERS and TEPL analysis of the MoS_2 sample transferred to a coverslip substrate. (a) APD image of PL intensity made using a bandpass filter with 1.81 to 1.78 eV spectral window. (b) Spectra collected with (red) and without (black) the PTTP nanoantenna showing a spectral enhancement of ~17× (A_1' peak) and PL enhancement of 5× (at 1.91 eV). (c) TEPL hyperspectral imaging, showing PL intensity centered at 1.80 eV spectral position. (d) Topography image acquired at the region showed on the dashed inset (c). (e) TEPL images of the intensity of neutral exciton peak at 1.82 eV. (f) TEPL spectra from two regions, circle and triangle, taken from image (e). (g,h) TEPL images of the neutral exciton peak position and fwhm. (i) The Raman spectra at the region of 180−720 cm^{-1} for the positions indicated in (f) showing the LA, E′, A_1', and 2LA peaks. (j,k,l) Hyperspectral images rendering the Raman peak area of the 2LA(448 cm^{-1}), A_1'(408 cm^{-1}) and LA(192 + 223 + 245) cm^{-1} peaks, respectively.

https://doi.org/10.1021/acs.jpcc.1c05510
J. Phys. Chem. C 2021, 125, 21011−21017

residues or dust deposited over the sample after the transfer process.

We also observed that the TEPL is intense (bright region) in the same region where the neutral exciton peak is relatively narrow and blue-shifted, Figures 3e, 3g, and 3h. These can be related to oxygen passivation induced by the power of the laser or strain effect.[51,52] Besides, we analyzed the TERS images at the same region shown in Figure 3d. The Raman peaks, around 300 and 500 cm^{-1}, were fitted to generate images of 2LA (Figure 3j), A_1' (Figure 3k), and LA (Figure 3l), where the color intensity renders the area of the peak. The same region observed as brighter in the PL image is where the Raman 2LA band is intense. On the other hand, the Raman A_1' and LA do not show consistent changes through this 2×2 μm area. The coupling between 2LA and neutral excitation is expected to be more robust when compared to A_1' and LA.[53,54] Therefore, the TERS results corroborate the observed increase of the neutral exciton contribution at the same brighter region seen on the TEPL intensity image. This exciting observation can be related to oxygen passivation induced by the laser power since the oxygen can be bond to the sites where sulfur vacancies are present. Another explanation for these results is the strain-induced effects, for which a decrease of PL intensity and the PL peak blue shift are expected on strained regions. It is essential to notice that we did not find any cracks, wrinkles, and polymer residues on the surface of the MoS_2 sample by TEPL or TERS analysis.

We carry over the triangle to a TEM grid to investigate the structural property, such as the crystallinity of monolayers MoS_2 after the etching-free transfer. A large SEM image is shown in Figure 4a. The hexagonal lattice structure typical for

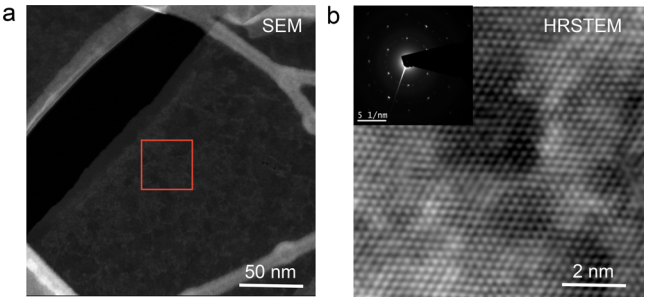

Figure 4. SEM and HRSTEM images of transferred monolayer MoS_2 to a TEM grid. (a) SEM image of a transferred triangle. (b) High-resolution STEM image of transferred MoS_2. The inset shows the electron diffraction along the [0001] zone axis, revealing the 6-fold symmetry of the {1100} reflection.

MoS_2 was preserved after transfer, as seen in the HRSTEM image, Figure 4b. Only Mo sites are visible due to the strong HAADF contrast of Mo atoms compared to lighter S atoms. The electron diffraction (inset) along the [0001] zone axis reveals the {1100} reflection's 6-fold symmetry. These images evidence that the proposed etching-free procedure preserves the crystallinity of as-grown MoS_2 samples.

CONCLUSIONS

In summary, we developed an etching-free transfer method for monolayers of MoS_2 and performed nanoimaging of transferred samples. The method involved polyurethane as a sacrifice layer. The polymer layer was peeled off from the substrate by tweezers and transferred to any substrate. Then, the polyurethane film was removed by dissolution in DMF. Using this method, we performed nanoimaging analysis on the transferred samples to a glass coverslip and a TEM grid by AFM, TERS, TEPL, SEM, and HRSTEM. Although oxygen passivation or strain-induced effects have been noted through the optical nanoimaging, we did not observe any cracks or wrinkles at the crystal, as well as no polymer residues. In general, the method integrally transfers monolayers of MoS_2 onto a target substrate, preserving the structural and optical properties. Our method can be used to transfer as-grown 2D-TMD to any arbitrary substrate.

ASSOCIATED CONTENT

Supporting Information

The Supporting Information is available free of charge at https://pubs.acs.org/doi/10.1021/acs.jpcc.1c05510.

Figure S1. Schematic diagram for the CVD synthesis. Figure S2. Photographs of the transfer steps. Figure S3. Additional optical images of transferred samples. Figure S4. SEM images of transferred samples. Figure S5. Raman and PL maps of the transferred sample. Figure S6. Raman and PL spectra of the before and after the transfer. (PDF)

AUTHOR INFORMATION

Corresponding Author

Victor Carozo − *Departamento de Física, Pontifícia Universidade Católica do Rio de Janeiro, Rio de Janeiro, RJ 22451900, Brasil;* orcid.org/0000-0002-0751-6435; Phone: +55 21 3527-1271; Email: vcarozo@puc-rio.br; Fax: +55 21 3527-1271

Authors

Syed Hamza Safeer − *Departamento de Física, Pontifícia Universidade Católica do Rio de Janeiro, Rio de Janeiro, RJ 22451900, Brasil;* orcid.org/0000-0003-3677-7340

Thiago L. Vasconcelos − *Divisao de Metrologia de Materiais, Instituto Nacional de Metrologia, Qualidade e Tecnologia (INMETRO), Duque de Caxias, Rio de Janeiro, RJ 25250020, Brasil*

Bruno S. Oliveira − *Divisao de Metrologia de Materiais, Instituto Nacional de Metrologia, Qualidade e Tecnologia (INMETRO), Duque de Caxias, Rio de Janeiro, RJ 25250020, Brasil*

Braulio Soares Archanjo − *Divisao de Metrologia de Materiais, Instituto Nacional de Metrologia, Qualidade e Tecnologia (INMETRO), Duque de Caxias, Rio de Janeiro, RJ 25250020, Brasil;* orcid.org/0000-0001-8145-7712

Michael Nazarkovsky − *Departamento de Quimica, Pontifícia Universidade Católica do Rio de Janeiro, Rio de Janeiro, RJ 22451900, Brasil*

Cecília Vilani − *Departamento de Quimica, Pontifícia Universidade Católica do Rio de Janeiro, Rio de Janeiro, RJ 22451900, Brasil*

Fernando Lazaro Freire − *Departamento de Física, Pontifícia Universidade Católica do Rio de Janeiro, Rio de Janeiro, RJ 22451900, Brasil*

Complete contact information is available at: https://pubs.acs.org/10.1021/acs.jpcc.1c05510

Author Contributions

All authors have given approval to the final version of the manuscript.

Notes

The authors declare no competing financial interest.

■ ACKNOWLEDGMENTS

S.H.S and V.C. acknowledge support from CNPq and FAPERJ grant numbers 304144/2018-5, 429773/2018-8, and E-26/010.000980/2019. S.H.S and V.C. acknowledge Flavio Garcia from CBPF for the access to SEM. F.L.F. acknowledges support from Conselho Nacional de Desenvolvimento Científico e Tecnológico (CNPq) (Processo CNPq 303283/2016-5), Instituto Nacional de Engenharia de Superfícies (INCT-INES) (Processo CNPq 465423/2014-0), and Fundação Carlos Chagas de Amparo á Pesquisa no Estado do Rio de Janeiro (FAPERJ) (Processo FAPERJ 210.167/2018). T.L.V. acknowledges support from CNPq (305881/2019-1 and 436381/2018-4) and MCTI (SibratecNano 21040). The authors acknowledge the use of the Materials Metrology Division, Instituto Nacional de Metrologia, Qualidade e Tecnologia (INMETRO). The authors are gratefull to R. S. Alencar for valuable inputs.

■ REFERENCES

(1) Geim, A. K.; Novoselov, K. S. The rise of graphene. *Nat. Mater.* **2007**, *6*, 183−191.
(2) Schwierz, F. Graphene transistors. *Nat. Nanotechnol.* **2010**, *5*, 487−496.
(3) Bilgin, I.; Liu, F.; Vargas, A.; Winchester, A.; Man, M. K. L.; Upmanyu, M.; Dani, K. M.; Gupta, G.; Talapatra, S.; Mohite, A. D.; et al. Chemical Vapor Deposition Synthesized Atomically Thin Molybdenum Disulfide with Optoelectronic-Grade Crystalline Quality. *ACS Nano* **2015**, *9*, 8822−8832.
(4) Wu, S.; Huang, C.; Aivazian, G.; Ross, J. S.; Cobden, D. H.; Xu, X. Vor-solid growth of high optical quality MoS_2 monolayers with near-unity valley polarization. *ACS Nano* **2013**, *7*, 2768−2772.
(5) Akinwande, D.; Huyghebaert, C.; Wang, C. H.; Serna, M. I.; Goossens, S.; Li, L. J.; Wong, H. S.; Koppens, F. H. Graphene and two-dimensional materials for silicon technology. *Nature* **2019**, *573*, 507−518.
(6) Bhimanapati, G. R.; Lin, Z.; Meunier, V.; Jung, Y.; Cha, J.; Das, S.; Xiao, D.; Son, Y.; Strano, M. S.; Cooper, V. R.; et al. Recent Advances in Two-Dimensional Materials beyond Graphene. *ACS Nano* **2015**, *9*, 11509−11539.
(7) Hossain, M. M.; Shabbir, B.; Wu, Y.; Yu, W.; Krishnamurthi, V.; Uddin, H.; Mahmood, N.; Walia, S.; Bao, Q.; Alan, T.; et al. Ultrasensitive WSe_2 field-effect transistor-based biosensor for label-free detection of cancer in point-of-care applications. *2D Mater.* **2021**, *8*, 045005.
(8) Liu, G.; Bao, X.; Dong, W.; Wei, Q.; Mu, H.; Zhu, W.; Wang, B.; Li, J.; Shabbir, B.; Huang, Y.; et al. Two-Dimensional $Bi_2Sr_2CaCu_2O_{8+\delta}$ Nanosheets for Ultrafast Photonics and Optoelectronics. *ACS Nano* **2021**, *15*, 8919−8929.
(9) Splendiani, A.; Sun, L.; Zhang, Y.; Li, T.; Kim, J.; Chim, C. Y.; Galli, G.; Wang, F. Emerging photoluminescence in monolayer MoS_2. *Nano Lett.* **2010**, *10*, 1271−1275.
(10) Radisavljevic, B.; Radenovic, A.; Brivio, J.; Giacometti, V.; Kis, A. Single-layer MoS_2 transistors. *Nat. Nanotechnol.* **2011**, *6*, 147−150.
(11) Liu, T.; Liu, S.; Tu, K. H.; Schmidt, H.; Chu, L.; Xiang, D.; Martin, J.; Eda, G.; Ross, C. A.; Garaj, S. Crested two-dimensional transistors. *Nat. Nanotechnol.* **2019**, *14*, 223−226.
(12) Gong, Y.; Carozo, V.; Li, H.; Terrones, M.; Jackson, T. N. High flex cycle testing of CVD monolayer WS_2 TFTs on thin flexible polyimide. *2D Mater.* **2016**, *3*, 021008.
(13) Choi, W.; Choudhary, N.; Han, G. H.; Park, J.; Akinwande, D.; Lee, Y. H. Recent development of two-dimensional transition metal dichalcogenides and their applications. *Mater. Today* **2017**, *20*, 116−130.
(14) Chhowalla, M.; Jena, D.; Zhang, H. Two-dimensional semiconductors for transistors. *Nat. Rev. Mater.* **2016**, *1*, 1−15.
(15) Shabbir, B.; Nadeem, M.; Dai, Z.; Fuhrer, M. S.; Xue, Q. K.; Wang, X.; Bao, Q. Long range intrinsic ferromagnetism in two dimensional materials and dissipationless future technologies. *Appl. Phys. Rev.* **2018**, *5*, 041105−1−15.
(16) Li, H.; Wu, J.; Yin, Z.; Zhang, H. Preparation and applications of mechanically exfoliated single-layer and multilayer MoS_2 and WSe_2 nanosheets. *Acc. Chem. Res.* **2014**, *47*, 1067−1075.
(17) Yuan, L.; Ge, J.; Peng, X.; Zhang, Q.; Wu, Z.; Jian, Y.; Xiong, X.; Yin, H.; Han, J. A reliable way of mechanical exfoliation of large scale two dimensional materials with high quality. *AIP Adv.* **2016**, *6*, 125201−1−7.
(18) Huang, Y.; et al. Universal mechanical exfoliation of large-area 2D crystals. *Nat. Commun.* **2020**, *11*, 5061.
(19) Ambrosi, A.; Pumera, M. The CVD graphene transfer procedure introduces metallic impurities which alter the graphene electrochemical properties. *Nanoscale* **2014**, *6*, 472−476.
(20) Lin, Z.; Thee, M. T.; Elías, A. L.; Feng, S.; Zhou, C.; Fujisawa, K.; Perea-López, N.; Carozo, V.; Terrones, H.; Terrones, M. Facile synthesis of MoS_2 and $Mo_xW_{1-x}S_2$ triangular monolayers. *APL Mater.* **2014**, *2*, 092514.
(21) Wang, X.; Gong, Y.; Shi, G.; Chow, W. L.; Keyshar, K.; Ye, G.; Vajtai, R.; Lou, J.; Liu, Z.; Ringe, E.; et al. Chemical vapor deposition growth of Crystalline Monolayer $MoSe_2$. *ACS Nano* **2014**, *8*, 5125−5131.
(22) Lee, Y. H.; Zhang, X. Q.; Zhang, W.; Chang, M. T.; Lin, C. T.; Chang, K. D.; Yu, Y. C.; Wang, J. T.; Chang, C. S.; Li, L. J.; et al. Synthesis of large-area MoS_2 atomic layers with chemical vapor deposition. *Adv. Mater.* **2012**, *24*, 2320−2325.
(23) Gong, Y.; Lin, J.; Wang, X.; Shi, G.; Lei, S.; Lin, Z.; Zou, X.; Ye, G.; Vajtai, R.; Yakobson, B. I.; et al. Vertical and in-plane heterostructures from WS_2/MoS_2 monolayers. *Nat. Mater.* **2014**, *13*, 1135−1142.
(24) Shivayogimath, A.; Thomsen, J. D.; Mackenzie, D. M.; Geisler, M.; Stan, R. M.; Holt, A. J.; Bianchi, M.; Crovetto, A.; Whelan, P. R.; Carvalho, A.; et al. A universal approach for the synthesis of two-dimensional binary compounds. *Nat. Commun.* **2019**, *10*, 2957.
(25) Safeer, S. H.; Moutinho, M. V. O.; Barreto, A. R. J.; Archanjo, B. S.; Pandoli, O. G.; Cremona, M.; da Costa, M. E.; Freire, F. L.; Carozo, V. Sodium-Mediated Low-Temperature Synthesis of Monolayers of Molybdenum Disulfide for Nanoscale Optoelectronic Devices. *ACS Applied Nano Materials* **2021**, *4*, 4172−4180.
(26) Liu, Z.; Amani, M.; Najmaei, S.; Xu, Q.; Zou, X.; Zhou, W.; Yu, T.; Qiu, C.; Birdwell, A. G.; Crowne, F. J.; et al. Strain and structure heterogeneity in MoS_2 atomic layers grown by chemical vapour deposition. *Nat. Commun.* **2014**, *5*, 5246.
(27) Gao, E.; Lin, S. Z.; Qin, Z.; Buehler, M. J.; Feng, X. Q.; Xu, Z. Mechanical exfoliation of two-dimensional materials. *J. Mech. Phys. Solids* **2018**, *115*, 248−262.
(28) Reina, A.; Son, H.; Jiao, L.; Fan, B.; Dresselhaus, M. S.; Liu, Z.; Kong, J. Transferring and Identification of Single- and Few-Layer Graphene on Arbitrary Substrates. *J. Phys. Chem. C* **2008**, *112*, 17741−17744.
(29) McCreary, K. M.; Hanbicki, A. T.; Singh, S.; Kawakami, R. K.; Jernigan, G. G.; Ishigami, M.; Ng, A.; Brintlinger, T. H.; Stroud, R. M.; Jonker, B. T. The effect of preparation conditions on raman and photoluminescence of monolayer WS_2. *Sci. Rep.* **2016**, *6*, 35154.
(30) Mlack, J. T.; Masih Das, P.; Danda, G.; Chou, Y. C.; Naylor, C. H.; Lin, Z.; López, N. P.; Zhang, T.; Terrones, M.; Johnson, A. T.; et al. Transfer of monolayer TMD WS_2 and Raman study of substrate effects. *Sci. Rep.* **2017**, *7*, 43037.
(31) Uwanno, T.; Hattori, Y.; Taniguchi, T.; Watanabe, K.; Nagashio, K. Fully dry PMMA transfer of graphene on h-BN using a heating/ cooling system. *2D Mater.* **2015**, *2*, 041002.

https://doi.org/10.1021/acs.jpcc.1c05510
J. Phys. Chem. C 2021, 125, 21011−21017

(32) Kathalingam, A.; Ajmal, H. M. S.; Ramesh, S.; Kim, H. S.; Kim, S. D.; Choi, S. H.; Yang, W.; Kim, K. K.; Kim, H. S. Poly(methyl methacrylate)-derived graphene films on different substrates using rapid thermal process: A way to control the film properties through the substrate and polymer layer thickness. *J. Mater. Res. Technol.* **2019**, *8*, 3752−3763.
(33) Zhang, T.; Fujisawa, K.; Granzier-Nakajima, T.; Zhang, F.; Lin, Z.; Kahn, E.; Perea-López, N.; Elías, A. L.; Yeh, Y. T.; Terrones, M. Clean Transfer of 2D Transition Metal Dichalcogenides Using Cellulose Acetate for Atomic Resolution Characterizations. *ACS Appl. Nano Mater.* **2019**, *2*, 5320−5328.
(34) Gurarslan, A.; Yu, Y.; Su, L.; Yu, Y.; Suarez, F.; Yao, S.; Zhu, Y.; Ozturk, M.; Zhang, Y.; Cao, L. Surface-energy-assisted perfect transfer of centimeter-scale monolayer and few-layer MoS_2 films onto arbitrary substrates. *ACS Nano* **2014**, *8*, 11522−11528.
(35) Castellanos-Gomez, A.; Buscema, M.; Molenaar, R.; Singh, V.; Janssen, L.; van der Zant, H. S. J.; Steele, G. A. Deterministic transfer of two-dimensional materials by all-dry viscoelastic stamping. *2D Mater.* **2014**, *1*, 011002.
(36) Zhang, F.; Erb, C.; Runkle, L.; Zhang, X.; Alem, N. Etchant-free transfer of 2D nanostructures. *Nanotechnology* **2018**, *29*, 025602.
(37) Xu, Z. Q.; Zhang, Y.; Lin, S.; Zheng, C.; Zhong, Y. L.; Xia, X.; Li, Z.; Sophia, P. J.; Fuhrer, M. S.; Cheng, Y. B.; et al. Synthesis and Transfer of Large-Area Monolayer WS_2 Crystals: Moving Toward the Recyclable Use of Sapphire Substrates. *ACS Nano* **2015**, *9*, 6178−6187.
(38) Frisenda, R.; Navarro-Moratalla, E.; Gant, P.; Pérez De Lara, D.; Jarillo-Herrero, P.; Gorbachev, R. V.; Castellanos-Gomez, A. Recent progress in the assembly of nanodevices and van der Waals heterostructures by deterministic placement of 2D materials. *Chem. Soc. Rev.* **2018**, *47*, 53−68.
(39) Lu, Z.; Sun, L.; Xu, G.; Zheng, J.; Zhang, Q.; Wang, J.; Jiao, L. Universal Transfer and Stacking of Chemical Vapor Deposition Grown Two-Dimensional Atomic Layers with Water-Soluble Polymer Mediator. *ACS Nano* **2016**, *10*, 5237−5242.
(40) Watson, A. J.; Lu, W.; Guimaraes, M.; Stoehr, M. Transfer of Large-Scale Two-Dimensional Semiconductors: Challenges and Developments. *2D Mater.* **2021**, *8*, 032001.
(41) Vilani, C.; Romani, E. C.; Larrudé, D. G.; Barbosa, G. M.; Freire, F. L. Direct transfer of graphene films for polyurethane substrate. *Appl. Surf. Sci.* **2015**, *356*, 1300−1305.
(42) Wang, X.; Wang, H.; Li, Y.; Xu, T.; Wang, W.; Cheng, J.; Shi, Z.; Yan, D.; Cui, Z. A novel functional polyurethane as a dielectric layer for organic thin-film transistors. *New J. Chem.* **2018**, *42*, 10969−10975.
(43) Avila, H. C.; Serrano, P.; Barreto, A. R. J.; Ahmed, Z.; de P. Gouvêa, C.; Vilani, C.; Capaz, R. B.; Marchiori, C. F. N.; Cremona, M. High hole-mobility of rrP3HT in organic field-effect transistors using low-polarity polyurethane gate dielectric. *Org. Electron.* **2018**, *58*, 33−37.
(44) Kim, D.; Kim, C.; Earmme, T. Polyurethane triblock copolymer gate dielectrics for low-voltage organic thin-film transistors. *J. Ind. Eng. Chem.* **2019**, *71*, 460−464.
(45) Yao, S.; Ren, P.; Song, R.; Liu, Y.; Huang, Q.; Dong, J.; O'Connor, B. T.; Zhu, Y. Nanomaterial-Enabled Flexible and Stretchable Sensing Systems: Processing, Integration, and Applications. *Adv. Mater.* **2020**, *32*, 1902343.
(46) Cançado, L. G.; Hartschuh, A.; Novotny, L. Tip-enhanced Raman spectroscopy of carbon nanotubes. *J. Raman Spectrosc.* **2009**, *40*, 1420−1426.
(47) Vasconcelos, T. L.; Archanjo, B. S.; Oliveira, B. S.; Valaski, R.; Cordeiro, R. C.; Medeiros, H. G.; Rabelo, C.; Ribeiro, A.; Ercius, P.; Achete, C. A.; et al. Plasmon-Tunable Tip Pyramids: Monopole Nanoantennas for Near-Field Scanning Optical Microscopy. *Adv. Opt. Mater.* **2018**, *6*, 1800528.
(48) Vasconcelos, T. L.; Archanjo, B. S.; Oliveira, B. S.; Silva, W. F.; Alencar, R. S.; Rabelo, C.; Achete, C. A.; Jorio, A.; Cançado, L. G. Optical Nanoantennas for Tip-Enhanced Raman Spectroscopy. *IEEE J. Sel. Top. Quantum Electron.* **2021**, *27*, 1−11.
(49) Oliveira, B. S.; Archanjo, B. S.; Valaski, R.; Achete, C. A.; Cançado, L. G.; Jorio, A.; Vasconcelos, T. L. Nanofabrication of plasmon-tunable nanoantennas for tip-enhanced Raman spectroscopy. *J. Chem. Phys.* **2020**, *153*, 114201.
(50) Mak, K. F.; He, K.; Lee, C.; Lee, G. H.; Hone, J.; Heinz, T. F.; Shan, J. Tightly bound trions in monolayer MoS_2. *Nat. Mater.* **2013**, *12*, 207−11.
(51) Rao, R.; Carozo, V.; Wang, Y.; Islam, A. E.; Perea-Lopez, N.; Fujisawa, K.; Crespi, V. H.; Terrones, M.; Maruyama, B. Dynamics of cleaning, passivating and doping monolayer MoS 2 by controlled laser irradiation. *2D Mater.* **2019**, *6*, 045031.
(52) He, X.; Li, H.; Zhu, Z.; Dai, Z.; Yang, Y.; Yang, P.; Zhang, Q.; Li, P.; Schwingenschlogl, U.; Zhang, X. Strain engineering in monolayer WS_2, MoS_2, and the WS_2/MoS_2 heterostructure. *Appl. Phys. Lett.* **2016**, *109*, 173105.
(53) Carvalho, B. R.; Malard, L. M.; Alves, J. M.; Fantini, C.; Pimenta, M. A. Symmetry-Dependent Exciton-Phonon Coupling in 2D and Bulk MoS_2 Observed by Resonance Raman Scattering. *Phys. Rev. Lett.* **2015**, *114*, 136403.
(54) Carvalho, B. R.; Wang, Y.; Mignuzzi, S.; Roy, D.; Terrones, M.; Fantini, C.; Crespi, V. H.; Malard, L. M.; Pimenta, M. A. Intervalley scattering by acoustic phonons in two-dimensional MoS_2 revealed by double-resonance Raman spectroscopy. *Nat. Commun.* **2017**, *8*, 14670.

https://doi.org/10.1021/acs.jpcc.1c05510
J. Phys. Chem. C 2021, 125, 21011−21017